Research Article | Vol. 13, No. 2 / 1 Feb 2022 / Biomedical Optics Express 620
Biomedical Optics EXPRESS

Polarization memory rate as a metric to differentiate benign and malignant tissues

DANIEL C. LOUIE,[1,2,3,4,*] LIOUDMILA TCHVIALEVA,[1,2,4] SUNIL KALIA,[1,2,4] HARVEY LUI,[1,2,4] AND TIM K. LEE[1,2,3,4]

[1]Department of Dermatology and Skin Science, University of British Columbia, Vancouver, BC V6T 1Z4, Canada
[2]Photomedicine Institute, Vancouver Coastal Health Research Institute, Vancouver, BC V6T 1Z4, Canada
[3]School of Biomedical Engineering, University of British Columbia, Vancouver, BC V6T 1Z4, Canada
[4]Departments of Cancer Control Research and Integrative Oncology, BC Cancer, Vancouver, BC V5Z 1L3, Canada
*daniel.louie@ubc.ca

Abstract: Non-invasive optical methods for cancer diagnostics, such as microscopy, spectroscopy, and polarimetry, are rapidly advancing. In this respect, finding new and powerful optical metrics is an indispensable task. Here we introduce polarization memory rate (*PMR*) as a sensitive metric for optical cancer diagnostics. *PMR* characterizes the preservation of circularly polarized light relative to linearly polarized light as light propagates in a medium. We hypothesize that because of well-known indicators associated with the morphological changes of cancer cells, like an enlarged nucleus size and higher chromatin density, *PMR* should be greater for cancerous than for the non-cancerous tissues. A thorough literature review reveals how this difference arises from the anomalous depolarization behaviour of many biological tissues. In physical terms, though most biological tissue primarily exhibits Mie scattering, it typically exhibits Rayleigh depolarization. However, in cancerous tissue the Mie depolarization regime becomes more prominent than Rayleigh. Experimental evidence of this metric is found in a preliminary clinical study using a novel Stokes polarimetry probe. We conducted *in vivo* measurements of 20 benign, 28 malignant and 59 normal skin sites with a 660 nm laser diode. The median *PMR* values for cancer vs non-cancer are significantly higher for cancer which supports our hypothesis. The reported fundamental differences in depolarization may persist for other types of cancer and create a conceptual basis for further developments in polarimetry applications for cancer detection.

1. Introduction

Tissue biopsy, the acknowledged gold standard for cancer detection, is based on the visualization of morphological changes in cancer tissue on a cellular level. Current optical imaging aims to offer non-invasive methods which could be automated and provide diagnostics *in vivo*. Several types of light-tissue interactions have generated a diversity of imaging techniques. For example, photographic, multispectral, narrow-band, fluorescence, light scattering spectroscopy, and multi-photon imaging exploits mostly absorption in endogenous chromophores whereas molecular scattering is of foremost importance in Raman, diffuse optical tomography, and diffuse reflectance [1]. Despite a wide variety of existing optical methods, a search for new approaches with different contrast mechanisms is under enduring attention. Coherence and polarization are optical properties connected to light phase and could create additional channels of information. The interaction of polarized light and biological tissue is a growing area in biomedical optics with a substantial development achieved recently [2,3]. The specially arranged polarization with optical angular momentum opens new perspectives for practical biomedical applications [4]. Coherent-domain optical metrology, which includes polarimetry, currently provides the highest

#446094 https://doi.org/10.1364/BOE.446094
Journal © 2022 Received 18 Oct 2021; revised 15 Dec 2021; accepted 21 Dec 2021; published 6 Jan 2022

Biomedical Optics EXPRESS

sensitivity and accuracy among optical techniques at the scale of micro-structural pathological changes occurring at the sub-cellular level [5,6]. Traditionally polarization has been used for optical gating, to contrast shallow photons which undergo a smaller number of scattering events against deeper ones [7]. To this point, the combination of polarized images visualizes skin pathology with enhanced contrast [8]. Recently, modification of tissue intrinsic polarization properties was linked to tissue pathological alterations which makes a polarimetry useful tool for skin [9–11], liver [12], breast [13–15], lung [16], prostate [17,18], and colon [19] cancer detection. The changes in polarization properties like depolarization, birefringence, and diattenuation are the subject of polarimetry. Depolarization is the most prominent effect when polarized light propagates in scattering media and exceeds birefringence and attenuation by an order of magnitude [20]. It is a direct result of scattering and rises quickly over the course of several scattering events. It is expected that the characteristic depolarization length within a medium is of the same order as the transport length and depends on bulk optical coefficients [21]. While bulk optical coefficients demonstrate some differences for cancer vs noncancerous tissues, this dissimilarity is not considered a reliable diagnostic criterion [22]. However, depolarization behaviour can be different even in tissue with the same bulk optical properties [23], which makes it a more reliable parameter for tissue differentiation. The most common metrics quantifying depolarization are the Degree of Polarization *(DOP)* and the Polarization Memory Rate *(PMR)*. These properties will be defined and explained in section 2. *PMR* is a relatively new polarization metric and its diagnostic potential was recently demonstrated though not fully explored. For example, *PMR* was able to separate pig skin damaged by irradiation from healthy tissue [24]. In the present paper we explore the diagnostic potential of *PMR* for skin cancer detection. We hypothesize that morphological changes in cancer cells will lead to a noticeable increase in *PMR* value for cancer tissue compared to benign.

2. Physical background

Polarization is the orientation of the tip of the electrical vector of an oscillating light wave. In the fully polarized case, this wave is modeled as an elliptical trajectory that includes linear and circular components. Light can also be depolarized, in which the oscillations are randomly oriented. The polarization state of light can be quantified through a Stokes vector S containing four Stokes parameters as per Eq. (1) [3,25].

$$S = \begin{bmatrix} S_0 \\ S_1 \\ S_2 \\ S_3 \end{bmatrix} = \begin{bmatrix} I_0 + I_{90} \\ I_0 - I_{90} \\ I_{45} - I_{135} \\ I_{RH} - I_{LH} \end{bmatrix} \tag{1}$$

Each of the Stokes parameters corresponds to the difference between two orthogonal components of polarization. S_0 is the total intensity of polarized light and can be calculated as sum of any two orthogonal components. S_1 is the difference between horizontally and vertically linear polarized components, S_2 is the difference between linear polarized components +45° and -45° from the horizontal, and S_3 is the difference in intensity between right- and left-hand circular polarized components. The Stokes parameters can be determined from six intensity measurements. In addition, due to the relationships between the Stokes parameters, it is possible to measure a Stokes vector using only four intensity measurements. From the Stokes vector, one can calculate the characteristics of the polarization ellipse and depolarization metrics such as the degree of polarization *(DOP)*, and its component parts degree of circular polarization (*DOCP)*, and degree

Biomedical Optics EXPRESS

of linear polarization (*DOLP*) as in Eq. (2) [3] [25]

$$DOCP = \frac{\sqrt{S_3^2}}{S_0},\ DOLP = \frac{\sqrt{S_1^2+S_2^2}}{S_0},\ DOP = \frac{\sqrt{S_1^2+S_2^2+S_3^2}}{S_0} \tag{2}$$

The most common metric used to quantify depolarization behavior is the Degree of Polarization (*DOP*), which represents the fraction of backscattered light that remains polarized. It ranges from 0 for fully depolarized to 1 for fully polarized light and could lie between 0 and 1, for partially polarized light. A non-negative form of *DOCP* is adopted in our model, noting that other conventions allow for negative *DOCP* of circular light to indicate helicity [26]. However, while *DOP* depends on tissue optical properties, it can also vary due to light source characteristics, initial light polarization, and detection geometry [27]. As a result, *DOP* is difficult to standardize across different tissue polarimetry machines. The metric we focus on in this paper is the Polarization Memory Rate (*PMR*), so named after the concept of polarization memory introduced in [28], which is the ability for light to remain polarized and forego decay as it travels through a medium. *PMR* as a measure of the relative rates of linear and circular polarization decay was explored as a metric separating Mie and Rayleigh scattering regimes in [29]. In the present paper, we will follow [24] where *PMR* is defined as the ratio of the *DOP* of the circular component of polarized light (*DOCP*) to the *DOP* of the linear component of polarized light (*DOLP)*, as in Eq. (3).

$$PMR = \frac{DOCP}{DOLP} \tag{3}$$

If the probing light has stronger circulation polarization memory it results in $PMR > 1$, in the case of the preservation of the linear polarization $PMR < 1$. As a relative measure, it is possible that this metric is more easily comparable between devices than *DOP*, and less affected by surface roughness [30]; though these relationships will need to be verified in future study.

3. Physical model

3.1. Scattering regime

Since depolarization occurs due to scattering it is important to introduce two basic scattering models, which can then lead to specific depolarization models. Small particles (where particle size < light wavelength) demonstrate isotropic scattering in the Rayleigh regime, whereas and large particles (where size > wavelength) have a large forward scattering component in the Mie regime [31]. The boundary between scattering regimes is evaluated by calculating the size parameter.

$$X = \frac{d\pi n_m}{\lambda} \tag{4}$$

where d is the diameter of a spherical scatterer, n_m is the refractive index of the surrounding media, and λ is the wavelength of the probing light [31]. Mie anisotropic scattering occurs when $X >> 1$, while Rayleigh isotropic scattering occurs when $X << 1$. Rayleigh and Mie regimes represent two fundamental physical models of scattering with different theory and outcomes, which also encompass the depolarization of light [32]. However, depolarization behaviour is not as closely linked to scatterer size. Due to other factors described below, it is possible to have Mie-sized particles display depolarization found in the Rayleigh regime. Therefore Rayleigh and Mie depolarization regimes must be independently identified. For qualitative identification of these two depolarization regimes, let us explore the mechanisms of depolarization using the concept of electromagnetic waves.

3.2. Depolarization mechanisms

Two mechanisms of depolarization, "geometrical" and "dynamical" are introduced in [33]. Geometrical depolarization is caused by changes in the polarization plane orientation as a

Biomedical Optics EXPRESS

wave propagates in the scattering media. The random trajectory change caused by scattering results in randomized orientations of the wave polarization plane, and this increased randomness causes light to depolarize. Dynamical depolarization is caused by changes in the complex amplitudes of cross-polarized wave components (those parallel and perpendicular to the scattering plane). This type of depolarization occurs as these amplitudes disperse after multiple scattering events. A key differentiating factor is that linear components of polarized light undergo both depolarization mechanisms whereas circular polarized components of light undergo only dynamical depolarization, due to circular polarization's independence from plane orientation due to axial symmetry.

3.3. Depolarization regime vs. scattering regime

To relate the model of depolarization mechanisms to the scattering regimes, it was shown [33] that the depolarization of light in anisotropic media composed of large Mie scatterers is dominated by geometrical depolarization. In this media, single scattering predominantly occurs in a forward direction, which more strongly affects polarization plane rotation than the amplitudes of cross polarized components. This leads to a dominance of geometrical over dynamical depolarization in the Mie anisotropic regime, resulting in a faster decay of the linear polarization component of light compared to circular per scattering event [28,34]. The opposite tendency is observed in the isotropic Rayleigh regime where forward and backward scattering have more equal possibility. Backward scattering will introduce an additional helicity flip in circular polarization, which results in a faster decay of circular polarized components relative to linear [26]. These differences in light depolarization make *PMR* useful in characterizing the Mie and Rayleigh scattering regimes. Mie media with relatively large scattered particles should have a predominant circular polarization memory with $PMR > 1$, and conversely Rayleigh media with relatively small scatterers is expected to preserve linear light better with $PMR < 1$ [29].

The scattering of light in biological tissue is a complex process involving particles with essentially different sizes and two types of scattering occurring simultaneously. Yet, it is possible to identify the average scattering regime by the value of the bulk anisotropy index g which approaches 1 and 0 for Mie and Rayleigh scattering respectively [31]. Most biological tissues demonstrate anisotropic scattering with g (in the visible region, 600 nm) in the diapason of 0.7-0.9 [35–37]. This is typical of scatterers in the Mie scattering regime and are expected to exhibit circular polarization memory with $PMR > 1$. However, recent studies show that colon, bladder, muscles, skin, liver, fat and many other tissues maintain linear polarization memory with $PMR < 1$ [19,24,38], which would indicate anomalous depolarization in the Rayleigh depolarization regime. Anomalous depolarization is a specific phenomenon that occurs due to a low relative refractive index between the scatterer and medium, as described in section 3.4 below. Note that the preservation of the linear polarization could also appear due to the backscattering observation mode [39]. Another important factor that could maintain linear polarization memory preferentially to circular polarization memory in tissue is the considerable number of small particles present in the extracellular matrix and cell compartments, like mitochondria, lysosomes, and collagen fibrils [19,40,41]. Ultimately, we expect that a combination of device geometry, ordinary depolarization from small particles, and anomalous depolarization from large particles contributes to the predominant Rayleigh depolarization [42].

Beyond the effect of malignancy on the cell nucleus, it is also necessary to regard stromal changes, such as the disordering of extracellular collagen. These changes are often observed in tissue polarimetry, visible through birefringence and diattenuation imaging channels [20,43], though they are less relevant to depolarization mechanisms [44]. As stated above, the scattering of light in biological tissue is complex and multifaceted, and as such the explanation offered by our model limits its scope to depolarization caused by changes in the cell nucleus and refractive indices.

Biomedical Optics EXPRESS

3.4. Anomalous depolarization

Anomalous depolarization behavior is linked to a low relative refractive index $m = n_{s/}n_m$, where n_s and n_m are the refractive indices of scatterers and of surrounding media respectively [45] [42]. The Mie and Rayleigh depolarization regimes are better separated using a reduced size parameter X' [42] dependent on m:

$$X' = (m - 1)X \tag{5}$$

The above cited work states that Mie media with X'<2.5 and sizes X >>1 will display Rayleigh depolarization with linear polarization memory, if (m-1)<<1. The relative refractive index of cell compartments mostly satisfies the condition for anomalous depolarization behaviour [46]. The depolarization areas are schematically shown in Fig. 1. Usual Rayleigh and Mie scattering regions occur the left and right of the indicated scattering regime boundary. To the right of the boundary, all scattering is in the Mie regime. However, depolarization regime is separated by a different axis, depicted in pink and blue respectively. The transition area between the two regimes is indicated in white. It is located under the borderline $X' = 2.5$ introduced in [42] and covers the transition and Mie scattering regions. To note, at higher m the depolarization regime boundary joins the scattering regime boundary.

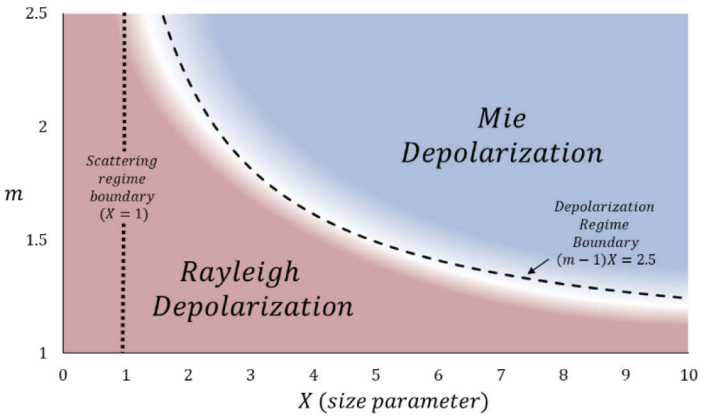

Fig. 1. The diagram of the two fundamental regimes of depolarization in terms of relative index of refraction m and size parameter X [42] . The Rayleigh and Mie depolarization zones are depicted in pink and blue correspondingly. The transitional area between two regimes indicated in white.

4. Evidence and literature

The theoretical support of our hypothesis can be obtained from published data. It is well-known that cancerous and precancerous cells present with a significant enlargement in nucleus diameter (increased X) and mass density of cell nuclei [47]. Cells with denser nuclei should have an increased n_s refractive index (which will increase m), and has been confirmed for colon [48], brain [49], and breast cancer [50]. Larger X and m could push the depolarization regime toward Mie depolarization, which is a change measurable with *PMR*.

For normal intestinal epithelial cells the diameters were obtained in the range of $d = 5.0 \pm 0.5$ µm with $m = 1.035$. For T84 intestinal malignant cells the corresponding values were $d = 9.8 \pm 1.5$ µm and $m = 1.040$ [47]. Taking into account the typical refractive index for cell cytoplasm $n_m = 1.37$ ($\lambda = 0.63$ µm) [46] and using Eq (4) and (5), we can evaluate the approximate size parameters for normal and cancerous nucleus as $X = 34 \pm 3$ µm and $X = 67 \pm 10$ µm correspondingly. Both numbers are much greater than 1 and link to the Mie scattering regime, as expected of biological

Biomedical Optics EXPRESS

tissue. However, the reduced size parameter for the normal cells X'=1.2 ± 0.1 is less than the boundary value 2.5 and linked to Rayleigh depolarization regime with $PMR < 1$. As for the cancerous cells, the reduced size parameter X'=2.7 ± 0.4 exceeds the boundary between two depolarization regimes which should lead to $PMR > 1$. Using refractive indexes of brain tissues measured in [49], assuming similar nucleus diameters, n_m, and following calculations shown for the first example, it is possible to set the same approximate size parameters for gray matter $X = 34$ ($d = 5.0$, $n_s = 1.39$, $n_m = 1.37$) and for glioblastoma $X = 67$ ($d = 9.8$, $n_s = 1.45$, $n_m = 1.37$). As in the case of intestinal epithelial cells, the numbers are associated with Mie scattering regime. Due to greater diversity of relative refractive indexes $m = n_{s/}n_m$ for brain tissue, the reduced size parameters are about X' =0.5 (Rayleigh depolarization, $PMR < 1$) for normal tissue and X' =3.9 for brain cancer (Mie depolarization, $PMR > 1$). These findings are summarized in Table 1. By the classical definition, one could define normal tissue and cancerous tissue as Mie scatterers. However, the new ranging based on the reduced size parameter X' describes cancerous tissue as obeying Mie while the non-cancerous tissue mostly following Rayleigh depolarization models. This fundamental shift could be evaluated by the Polarization Memory Rate which exposes the relative decay of circular vs linear polarizations at a time when light propagates in a tissue.

Table 1. Summary of benign and malignant tissue differences in literature

Ref	Tissue type	d (μm)	m	X	X'	Scattering Regime	Depolarization Regime	PMR
[47]	Epithelial intestine	5.0	1.035	34	1.2	Mie	Rayleigh	<1
[47]	Malignant intestine	9.8	1.040	67	2.7	Mie	Mie	>1
[49]	Gray matter	5.0	1.015	34	0.5	Mie	Rayleigh	<1
[49]	Glioblastoma	9.8	1.058	67	3.9	Mie	Mie	>1

5. Experimental background and methods

Practical implementation of polarimetry for bulk tissue cancer detection has been explored through a variety of methods [3], where examples of measurement schemes are often tailored to the intended target site be they *ex vivo* [51,52] or *in vivo* [43,53]. As shown in each example, complete Mueller matrix measurement is now the most common polarimetric analysis, allowing for the calculation of a large variety of depolarization metrics. Any of these metrics, or a combination thereof, may be the optimal method to measure the proposed fundamental shift in depolarization between benign and malignant tissues. Recognizing that PMR is one of many depolarization metrics, the present study measures PMR to take advantage of the simplicity and rapid measurement speed of Stokes vector polarimetry. The more lightweight instrumentation of Stokes vector polarimetry offers it greater flexibility for applications on *in vivo* body sites other than skin, and ease of implementation into the clinical workflow. In addition, our instrumentation follows a line of research measuring polarization speckle. Mueller matrix imaging systems, such as in [54], optimize their images by employing mechanisms to erase speckle. With an aim to embrace speckle, a short measurement time on the order of 5 ms is required to eliminate the effect of movement when measuring a speckle pattern *in vivo*. It is a prominent future goal to measure the Mueller matrix in tandem with speckle, and to further investigate the fundamental depolarization shift through a Mueller matrix analysis.

The *in vivo* measurements in this study were taken by a handheld one-shot Stokes polarimetry probe shown in Fig. 2. This device offers rapid Stokes vector measurements, and includes the ability to alternate between linear and circular initial polarization states. In the operational geometry of this probe, the backscattered laser light from the target site forms a far-field speckle pattern in the detector plane, which is expected to be statistically uniform over the four detectors. Rather than four division-in-time measurements at one point in space, measurement

Biomedical Optics EXPRESS

time is decreased by employing four division-in-space measurements at one point in time. The polarization state analyzer (PSA) is comprised of four photodiodes with film polarizers (Bolder Vision Optik) placed in front. A polarization state generator (PSG) comprised of a wire grid polarizer and removable quarterwave plate film was used to maintain the specific polarization of the diode laser (660 nm, 120 mW, Thorlabs, HL6545MG) in either linear or right-hand circular polarization states. The diode laser is oriented with respect to the PSG such that a maximum intensity is transmitted through the system. The device is aligned on a skin target through the use of an adhesive sticker commonly used identify points of interest in dermatological practice. The maximum outer dimensions of the probe are 20 cm in length and 5 cm in diameter. The acquisition time is 4.7 milliseconds. More details on the probe construction and operation can be found in [55].

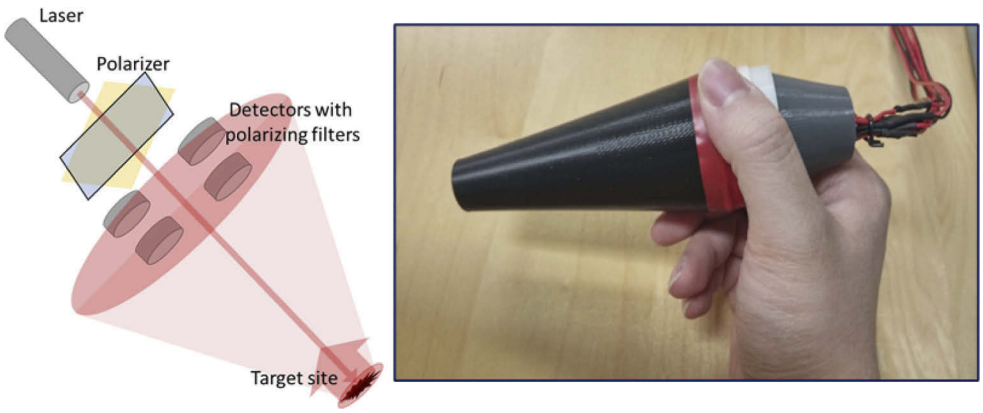

Fig. 2. The portable polarization probe, diagram and photograph.

6. Experimental results

For the experimental validation we have measured *PMR* for skin lesions *in vivo*. Skin is an easily accessible organ providing an opportunity to explore cancerous lesions, benign lesions, and normal healthy skin tissue. The latter two tissue types are both examples of non-cancerous morphology. After building a Stokes polarization probe, we conducted a preliminary clinical study involving 71 volunteer patients at the Vancouver General Hospital Skin Care Centre in Vancouver, Canada. The study was approved by University of British Columbia research ethical board, H06-&0281 and includes 6 malignant melanoma (MM), 14 basal cell carcinoma (BBC), 8 squamous cell carcinoma (SCC), 9 actinic keratosis (AK), 5 benign nevus (BN), 15 seborrheic keratosis (SK), and 59 normal skin cases. The diagnoses of malignant cases were pathologically proven. Skin sites were grouped in to three categories: cancer lesions (28), benign lesions (20) and normal skin sites taken contralateral to the lesion (59). Actinic Keratosis was not grouped as it is an intermediate pre-cancerous lesion. Using the Stokes probe (described in Methods), we measured *DOCP* and *DOLP* and calculated *PMR* for each case. The *PMR* values for the each lesion type, as well as grouped categories of cancer (MM, BCC, SCC), benign (BN, SK) and normal skin sites are shown in Fig. 3.

Most points have *PMR* values less than 1 indicating Rayleigh depolarization, however the measurements from cancerous lesions detect higher *PMR* values, indicating a shift toward Mie depolarization. The *PMR* measurements for the benign tissue pathology are similar to the normal skin. The benign pathologies and healthy tissues have close mean *PMR* values. Most *PMR* data for benign lesions are smaller than for skin cancer. Most of the points from cancerous lesions, and in particular MM, have *PMR* values closer to or greater than one than the benign lesion

Biomedical Optics EXPRESS

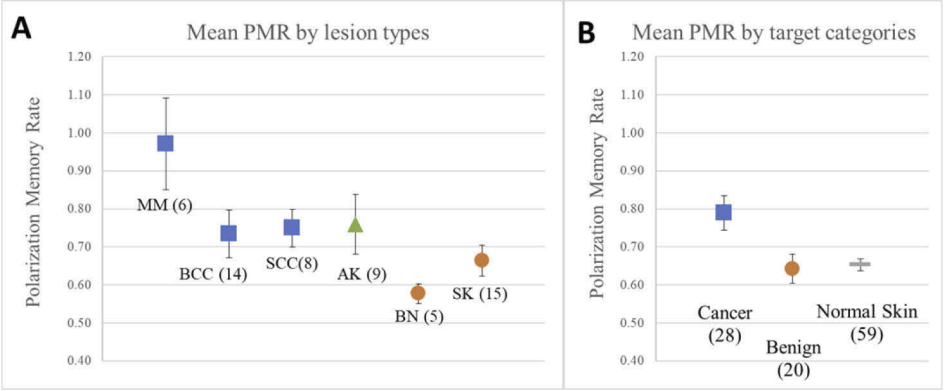

Fig. 3. Mean and standard error shown for each type of tested lesion (A), and categories of cancer, benign, and normal skin (B).

points, which demonstrates the approach to the Mie depolarization limit. The median *PMR* for cancer is greater than the median *PMR* for non-cancerous skin sites. In addition, measurements from actinic keratosis, which is an intermediate pre-cancer lesion, lies between the cancerous and benign categories. Because the data are not normally distributed (according to a Shapiro-Wilk test) a non-parametric Mann-Whitney U-Test was employed to find p-value 0.018 for cancerous vs benign lesions and 0.005 for cancerous lesions vs. normal skin sites from benign lesion patients. This skin lesion data indicates that *PMR* could potentially detect specific cancer pathology.

The whisker plot in Fig. 4 displays median values and inter-quartile range. Visually similar pairs of MM-BN and MM-SK images are shown with their *PMR* values indicated. The MM that resembles SK and BN could result in misdiagnosis of deadly skin cancer by practitioners.

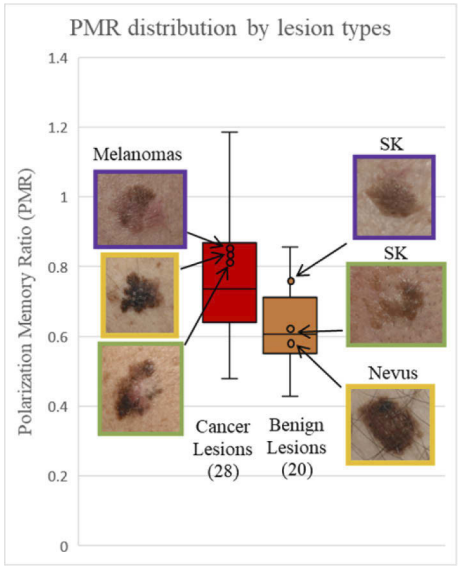

Fig. 4. Whisker plot of cancerous and benign categories indicating medians and interquartile range. Enhanced markers indicate pairs (Malignant Melanoma-Nevus and Malignant Melanoma-Seborrheic Keratosis) with visual similar clinical presentation. The corresponding images for MM are on the left and benign lesions are on the right.

Biomedical Optics EXPRESS

The results of the preliminary study validate the potential of Polarization Memory Rate as a metric for cancer differentiation. *PMR* demonstrates a significant 20% increase in median values for cancerous lesions compared to benign lesions which indicates behavior closer to the Mie depolarization regime. However, most of the measured *PMR* values for cancer comply with Rayleigh depolarization limit. In the Discussion section we will explore the factors influencing *PMR* and address the reasons why we primarily observe *PMR* less than one.

7. Discussion

7.1. Discussion of results

As is seen in Fig. 4, most measurements have $PMR < 1$, indicating the Rayleigh depolarization regime even theoretically we expect *PMR* points appearing in Mie region. There are a few possible reasons. A first factor reducing *PMR* might be the wavelength of the laser. The red diode laser with wavelength 660 nm has penetration depth on the order of a millimeter [56] and the emerging light spot of a few millimeters. Though thickness and depth data was not collected for all lesions in this study (as the benign lesions were not biopsied), the Breslow thicknesses of the collected melanoma lesions were each 1.5 mm or below. The majority of cancerous lesions examined in this study were subjects of early detection by dermatologists and the majority can be expected to be thin or superficial. As such, the propagating trajectories likely surpass the lesion volume adding a significant portion of the healthy tissue to the total signal. Under such circumstances the backscattering light will possibly obey the Rayleigh depolarization regime on average, as is typical of healthy skin. To address another aspect of geometry, we expect that lesion inhomogeneity would have only a minor contribution to the measurement, as the collected field is comprised of light emerging from a total volume that surpasses that of the lesion.

The second reason for the observed Rayleigh depolarization could be connected to a non-even distribution of depolarization over the backscattered area. This is not connected to sample inhomogeneity, but rather the general behaviour of depolarization in backscattering geometry. Both experimental and MC simulations show that for Mie depolarization media there is a local increase in linear polarization memory at central zones of the emerging spot [39]. The size of the anomalous Rayleigh depolarization area is about the transport mean free path of the turbid media and is located at the central area with maximal backscattered intensity. In this case the central backscattering signal with strong linear polarization memory might contribute to the total signal as well. These *PMR* reducing factors are mostly related to the detector placement within the probe geometry to ensure symmetrical detection of a uniform field. To note, this aspect of detection geometry is uniquely subject to user errors. A non-perpendicular orientation angle of the device with the target could result in non-symmetry when observing the backscattered field, resulting in further distortions. Finding the optimal light source wavelength for penetration control, and a device scheme resistant to orientation variance will be a future engineering pursuit.

However, even under these unfavorable experimental conditions, the *PMR* demonstrates some diagnostic ability linked to the specific morphological modifications in cancer cells. We assume that this is the result of a reasonable choice of the laser type and probe geometry. Choosing coherent laser light as the light source for this polarimetry device results in the formation of a stochastic interference pattern (speckle pattern) on the detector area. Speckles were initially treated as a noise in many imaging techniques, but speckle patterns contain additional information due to its encoding of light phase modifications, and recently has proven to have potential for medical diagnostics [57] becoming a quickly developed area in coherent optics [58]. Describing the components of a speckle pattern, each bright area (speckle) has an individual state of polarization *(SOP)* which is elliptical in general, but the parameters and orientation of the polarization ellipses may vary from speckle to speckle forming a polarization speckle pattern [59]. The ability to evaluate skin lesions using speckle patterns has been demonstrated [60], though their discriminative ability has strongly been linked to the lesion's surface roughness

Biomedical Optics EXPRESS

[61]. Indeed, the influence of surface roughness on the *DOP* measurements of the probe used in this study has been explored [11], and there is a negative correlation between surface roughness and *DOP*. However, a subsequent examination of roughness on *PMR*, a metric comprised of two relative *DOP* measurements, indicates a mitigation of surface roughness's influence on measurements [30], though this mechanism is still to be explored in detail. To embrace speckle, and the sensitivity it offers to our measurements, it is required for us to design probe with speckle behavior in mind.

7.2. Influence of speckle on results

There are three factors influencing polarization speckle: the light source, the scattering tissue, and the geometry of the device. Enhancing the detection of the biological markers of interest, the first and third factors should be carefully addressed. Polarization is a statistical phenomenon mutually connected with light coherence [62]. Because polarization and coherence correlation functions are of the same scale, light depolarization occurs at propagating distances comparable to light decorrelation which is of the order of the temporal coherence length [63]. Most photons with trajectories close to the coherence length will participate in polarization speckle formation, while the deeper photons will produce a uniform intensity bias. In order to convey relevant tissue information, the average photon path length in tissue must match the order of the temporal coherence length of the light source [64], and therefore we require a laser with a coherence length of a few millimeters to match the expected skin depolarization length [56]. In our probe we use a low coherence diode laser with the coherence length ~3 mm. The emerging light will be partially coherent and partially polarized to produce an informative value of *DOP* between 0 and 1. The diameter of the laser beam and the geometrical characteristics of the detection scheme define the light spatial coherence length which is about the average size of polarization speckle [65]. The amount of speckle on the detector area (equal to the area divided by a spatial coherence length) should be optimized. As shown in [66] the spatial degree of polarization depends on distribution of individual speckle *SOP*s over the speckle field. Therefore, if the number of speckles is high, in the case of single point measurements (as is the case with photodiode detectors) the spatial averaging over detector area could affect the measured *DOP* and degrade the information about tissue. Alternatively, if the number of speckles is low, the device will measure the average light intensity, *DOP,* and *PMR* with a large error which is inversely proportional to the square root of the number of speckles [67]. For the future optimization of the spatial coherence length of the laser field we should map the spatial distributions for *DOP(x,y)* and *PMD(x,y)* and explore their statistical moments.

8. Conclusion

Our hypothesis is that morphological changes in cancer cells will lead to a noticeable increase in *PMR* value for cancer tissue compared to benign. This is due to the difference in depolarization regime displayed by the scattering in benign and malignant cells. Our results present a numerical validation of this hypothesis based on published data and experimental validation based on measurements on skin tissue *in vivo*. Having chosen human skin as a convenient and easily accessible object, we designed a handheld polarization probe and conducted a preliminary clinical study including malignant lesions, benign lesions, and non-lesion skin sites. We discovered a statistically significant increase in *PMR* for malignant lesions relative to non-malignant sites, indicating that depolarization in skin cancer compared to non-cancerous tissues approaches the Mie depolarization regime. However, we recognize that this study is in its earliest stage, and we propose further testing to determine the extent to which this ultimate difference in *PMR* is measurable. We posit that this difference may be measurable in types of cancer beyond skin, to create a conceptual basis on which to advance the greater field of medical polarimetry.

Biomedical Optics EXPRESS

Funding. VGH and UBC Hospital Foundation; Canadian Dermatology Foundation; BC Cancer Foundation; Natural Sciences and Engineering Research Council of Canada (2017-04932); Canadian Melanoma Foundation.

Acknowledgements. This work is supported in part by grants from the BC Cancer Foundation, Canadian Melanoma Foundation, Canadian Dermatology Foundation, NSERC, and VGH and UBC Hospital Foundation. We thank all our study participants, and the clinical staff at the Vancouver General Hospital Skin Care Centre for their time and other contributions to this project.

Disclosures. The authors declare no relevant conflicts of interest.

Data Availability. Data underlying the results presented in this paper contains confidential patient information and are not publicly available at this time, but may be obtained from the authors upon reasonable request.

References

1. D. J. Waterhouse, C. R. M. Fitzpatrick, B. W. Pogue, J. P. B. O'Connor, and S. E. Bohndiek, "A roadmap for the clinical implementation of optical-imaging biomarkers," Nat. Biomed. Eng. **3**(5), 339–353 (2019).
2. J. C. Ramella-Roman, I. Saytashev, and M. Piccini, "A review of polarization-based imaging technologies for clinical and preclinical applications," J. Opt. **22**(12), 123001 (2020).
3. C. He, H. He, J. Chang, B. Chen, H. Ma, and M. J. Booth, "Polarisation optics for biomedical and clinical applications: a review," *Light: Sci. Appl.* 10(194), (2021).
4. I. Meglinski, T. Novikova, and K. Dholakia, "Polarization and Orbital Angular Momentum of Light in Biomedical Applications: feature issue introduction," Biomed. Opt. Express **12**(10), 6255–6258 (2021).
5. J. Qi and D. Elson, "Mueller polarimetric imaging for surgical and diagnostic applications: A review," J. Biophotonics **10**(10), 950–982 (2017).
6. V. V. Tuchin, L. Wang, and D. A. Zimnyakov, *Optical Polarization in Biomedical Applications* (Springer-Verlag Berlin Heidelberg, 2006).
7. L. V. Wang, G. L. Coté, and S. L. Jacques, "Special section guest editorial: tissue polarimetry," J. Biomed. Opt. **7**(3), 278 (2002).
8. S. L. Jacques, J. C. Ramella-Roman, and K. Lee, "Imaging skin pathology with polarized light," J. Biomed. Opt. **7**(3), 329–340 (2002).
9. P. Ghassemi, P. Lemaillet, T. Germer, J. Shupp, S. Venna, M. Boisvert, K. Flanagan, M. Jordan, and J. Ramella-Roman, "Out-of-plane Stokes imaging polarimeter for early skin cancer diagnosis," J. Biomed. Opt. **17**(7), 760141 (2012).
10. J. F. do Boer, C. K. Hitzenberger, and Y. Yasumo, "Polarization sensitive optical coherence tomography - a review," Biomed. Opt. Express **8**(3), 1838–1873 (2017).
11. D. C. Louie, J. Phillips, L. Tchvialeva, S. Kalia, H. Lui, W. Wang, and T. Lee, "Degree of optical polarization as a tool for detecting melanoma: proof of principle," J. Biomed. Opt. **23**(12), 1 (2018).
12. Y. Wang, H. He, J. Chang, S. Lui, M. Li, N. Zeng, J. Wu, and H. Ma, "Mueller matrix microscope: a quantitative tool to facilitate detection and fibrosis scorings of liver cirrhosis and cancer tissues," J. Biomed. Opt. **21**(7), 71112 (2016).
13. R. Patel, A. Khan, R. Quinlan, and A. Yaroslavsky, "Polarization-sensitive multimodal imaging for detecting breast cancer," Cancer Res. **74**(17), 4685–4693 (2014).
14. M. Villiger, D. Lorenser, R. McLaughlin, B. Quirk, R. Kirk, B. Bouma, and D. Sampson, "Deep tissue volume imaging of birefringence through fibre-optic needle probes for the delineation of breast tumour," Sci. Rep. **6**(1), 28771 (2016).
15. A. Golaraei, L. Kontenis, R. Cisek, D. Tokarz, S. Done, B. Wilson, and V. Barzda, "Changes of collagen ultrastructure in breast cancer tissue determined by second-harmonic generation double Stokes-Mueller polarimetric microscopy," Biomed. Opt. Express **7**(10), 4054 (2016).
16. B. Kunnen, C. Macdonald, A. Doronin, S. Jacques, M. Eccles, and I. Meglinski, "Application of circularly polarized light for non-invasive diagnosis of cancerous tissues and turbid tissue-like scattering media," J. Biophotonics **8**(4), 317–323 (2015).
17. V. Ushenko, A. Sdobnov, A. Syvokorovskava, A. Dubolazov, O. Vanchulyak, A. Ushenko, Y. Ushenko, M. Gorsky, M. Sidor, A. Bykov, and I. Meglinski, "3D mueller-matrix diffusive tomography of polycrystalline blood films for cancer diagnosis," Photonics **5**(4), 54 (2018).
18. V. A. Ushenko, B. T. Hogan, A. Dubolazov, G. Piavchenko, S. L. Kuznetsov, A. G. Ushenko, Y. O. Ushenko, M. Gorsky, A. Bykov, and I. Meglinski, "3D Mueller matrix mapping of layered distributions of depolarisation degree for analysis of prostate adenoma and carcinoma diffuse tissues," Nat. Rev. Cancer **11**(1), 5162 (2021).
19. T. Novikova, A. Pierangelo, A. De Martino, A. Benali, and P. Validire, "Polarimetric imaging for cancer diagnosis and staging," Opt. Photonics News **23**(10), 26–33 (2012).
20. N. Ghosh and I. Vitkin, "Tissue polarimetry: concepts, challenges, applications, and outlook," J. Biomed. Opt. **16**(11), 110801 (2011).
21. V. Tuchin, *Tissue Optics Light Scattering Methods and Instruments for Medical Diagnosis* (SPIE, 2000).
22. A. Garcia-Uribe, J. Zou, M. Duvic, J. H. Cho-Vega, V. Prieto, and L. Wang, "In vivo diagnosis of melanoma and nonmelanoma skin cancer using oblique incidence diffuse reflectance spectrometry," Cancer Res. **72**(11), 2738–2745 (2012).
23. A. Manzoor, S. Alali, A. Kim, M. F. G. Wood, M. Ikram, and I. A. Vitkin, "Do different turbid media with matched bulk optical properties also exhibit similar polarization properties?" Biomed. Opt. Express **2**(12), 3248–3258 (2011).

Biomedical Optics EXPRESS

24. F. Boulvert, Y. Piderriere, G. Le Brun, B. Le Jeune, and J. Cariou, "Comparison of entropy and polarization memory rate behavior through a study of weakly-anisotropic depolarizing biotissues," Opt. Commun. **272**(2), 534–538 (2007).
25. A. Vitkin, N. Ghosh, and A. De Martino, "Tissue Polarimetry," in *Photonics: Scientific Foundations, Technology and Applications*, Volume IV (John Wiley & Sons, Inc., 2015), pp. 203–321.
26. M. D. Singh and I. A. Vitkin, "Discriminating turbid media by scatterer size and scattering coefficient using backscattered linearly and circularly polarized light," Biomed. Opt. Express **12**(11), 6831–6843 (2021).
27. C. Amra, M. Zerrad, L. Siozade, G. Georges, and C. Deumié, "Partial polarization of light induced by random defects at surfaces or bulks," Opt. Express **16**(14), 10372–10354 (2008).
28. F. C. MacKintosh, J. X. Zhu, D. J. Pine, and D. A. Weitz, "Polarization memory of multiply scattered-light," Phys. Rev. B **40**(13), 9342–9345 (1989).
29. D. Bicout, C. Brosseau, A. Martinez, and J. Schmitt, "Depolarization of multiply scattered waves by spherical diffusers: Influence of the size parameter," Phys. Rev. E **49**(2), 1767–1770 (1994).
30. L. Tchvialeva, D. C. Louie, Y. Wang, S. Kalia, H. Lui, and T. K. Lee, "Polarization-based skin cancer detection in vivo," SPIE Proceedings Fifteenth International Conference on Correlation Optics, 2021.
31. A. Ishimaru, *Wave Propagation and Scattering in Random Media* (Academic Press, 1978.)
32. L. F. Rojas-Ochoa, D. Lacoste, R. Lenke, P. Schurtenberger, and F. Scheffold, "Depolarization of backscattered linearly polarized light," J. Opt. Soc. Am. **21**(9), 1799–1804 (2004).
33. E. E. Gorodnichev, A. I. Kuzolev, and D. B. Rogozkon, "Multiple scattering of polarized light in a turbid medium," J. Exp. Theor. Phys. **104**(2), 319–341 (2007).
34. G. Lewis, D. Jordan, and J. Roberts, "Backscattering target detection in a turbid medium by polarization discrimination," Appl. Opt. **38**(18), 3937–3944 (1999).
35. A. N. Bashkatov, E. A. Genina, and V. V. Tuchin, "Tissue Optical Properties," in *Handbook of Biomedical Optics* (Taylor & Francis Group,2011), pp. 67–100.
36. A. N. Bashkatov, E. A. Genina, V. Kochubey, V. S. Rubtsov, E. A. Kolesnikova, and V. V. Tuchin, "Optical properties of human colon tissues in the 350–2500 nm spectral range," Quantum Electron. **44**(8), 779–784 (2014).
37. S. L. Jacques, "Optical properties of biological tissues: a review," Phys. Med. Biol. **58**(11), R37–R61 (2013).
38. V. Sankaran, J. Walsh, and D. Maitland, "Comparative study of polarized light propagation in biologic tissues," J. Biomed. Opt. **7**(3), 300–306 (2002).
39. X. Wang, J. Lai, Y. Song, and Z. Li, "The anomalous depolarization anisotropy in the central backscattering area for turbid medium with Mie scatterers," J. Opt. **20**(5), 55601 (2018).
40. C. A. Nader, R. Nassif, F. Pellen, B. Le Jeune, G. Le Brun, and M. Abboud, "Influence of size, proportion, and absorption coefficient of spherical scatterers on the degree of light polarization and the grain size of speckle pattern," Appl. Opt. **54**(35), 10369–10375 (2015).
41. C. M. Macdonald, S. L. Jacques, and I. V. Meglinski, "Circular polarization memory in polydisperse scattering media," Phys. Rev. E **91**(3), 33204 (2015).
42. N. Ghosh, P. Gupta, A. Pradhan, and S. Majumder, "Anomalous behavior of depolarization of light in a turbid medium," Phys. Lett. A **354**(3), 236–242 (2006).
43. J. Chue-Sang, N. Holness, M. Gonzalez, J. Greaves, I. Saytashev, S. Stoff, A. Gandjbakhche, V. V. Chernomordik, G. Burkett, and J. C. Ramella-Roman, "Use of Mueller matrix colposcopy in the characterization of cervical collagen anisotropy," J. Biomed. Opt. **23**(12), 121605 (2018).
44. A. Vahidnia, K. Madanipour, R. Abedini, R. Karimi, J. Sanderson, Z. Zare, and P. Parvin, "Quantitative polarimetry Mueller matrix decomposition for diagnosing melanoma and non-melanoma human skin cancer," OSA Continuum **4**(11), 2862–2875 (2021).
45. A. D. Kim and M. Moscoso, "Influence of the relative refractive index on the depolarization of multiply scattered waves," Phys. Rev. E **64**(2), 26612 (2001).
46. P. Y. Liu, L. K. Chin, W. Ser, H. F. Chen, C. M. Hsieh, C. H. Lee, K. B. Sung, T. C. Ayi, P. H. Yap, B. Liedberg, K. Wang, T. Bourouina, and Y. Leprince-Wang, "Cell refractive index for cell biology and disease diagnosis: past, present and future," Lab Chip **16**(4), 634–644 (2016).
47. L. Perelman, "Optical diagnostic technology based on light scattering spectroscopy for early cancer detection: expert review of medical devices," Expert Rev. Med. Devices **3**(6), 787–803 (2006).
48. R. S. Gurjar, V. Backman, L. T. Perelman, I. Georgakoudi, K. Badizadegan, I. Itzkan, R. R. Dasari, and M. S. Feld, "Imaging human epithelial properties with polarized light-scattering spectroscopy," Nat. Med. **7**(11), 1245–1248 (2001).
49. T. Biswas and T. Luu, "In vivo MR measurement of refractive index, relative water content and T2 relaxation time of various brain lesions with clinical application to discriminate brain lesions," *The Internet Journal of Radiology* 13(1), (2009).
50. Z. Wang, K. Tangella, A. Kajdacsy-Balla, and G. Popescu, "Tissue refractive index as marker of disease," J. Biomed. Opt. **16**(11), 116017 (2011).
51. S. Alali and I. A. Vitkin, "Polarized light imaging in biomedicine: emerging Mueller matrix methodologies for bulk tissue assessment," J. Biomed. Opt. **20**(6), 61104 (2015).
52. J. Qi and D. S. Elson, "A high definition Mueller polarimetric endoscope for tissue characterisation," Sci. Rep. **6**(1), 25953 (2016).

Biomedical Optics EXPRESS

53. B. Varin, J. Rehbinder, J. Dellinger, C. Heinrich, M. Torzynski, C. Spenlé, D. Bagnard, and J. Zallat, "Monitoring subcutaneous tumors using Mueller polarimetry: study on two types of tumors," Biomed. Opt. Express **12**(10), 6055–6065 (2021).
54. O. Rodríguez-Núñez, P. Schucht, E. Hewer, T. Novikova, and A. Pierangelo, "Polarimetric visualization of healthy brain fiber tracts under adverse conditions: ex vivo studies," Biomed. Opt. Express **12**(10), 6674–6685 (2021).
55. D. C. Louie, L. Tchvialeva, S. Kalia, H. Lui, and T. K. Lee, "Constructing a portable optical polarimetry probe for in-vivo skin cancer detection," *J. Biomed. Opt.* 26(3) (2021).
56. X. Guo, M. F. G. Wood, and A. Vitkin, "Monte Carlo study of pathlength distribution of polarized light in turbid media," Opt. Express **15**(3), 1348–1360 (2007).
57. A. Ushenko, A. Sdobnov, A. Dubolazov, M. Gritsuk, Y. Ushenko, A. Bykov, and I. Meglinski, "Stokes-correlometry analysis of biological tissues with polycrystalline structure," IEEE J. Sel. Top. Quantum Electron. **25**(1), 1–12 (2019).
58. C. Zhang, S. Horder, T. K. Lee, and W. Wang, "Development of polarization speckle based on random polarization phasor sum," J. Opt. Soc. Am. A **36**(2), 277–282 (2019).
59. M. Takeda, W. Wang, and S. G. Hanson, "Polarization speckles and generalized Stokes vector wave: a review," Proc. SPIE 7387, 73870V (2010).
60. L. Tchvialeva, G. Dhadwal, H. Lui, S. Kalia, H. Zeng, D. I. McLean, and T. K. Lee, "Polarization speckle imaging as a potential technique for in vivo skin cancer detection," J. Biomed. Opt. **18**(6), 61211 (2012).
61. L. Tchvialeva, H. Zeng, I. Markhvida, D. I. McLean, H. Lui, and T. K. Lee, "Skin roughness assessment," in *New Developments in Biomedical Engineering* (Intech, 2010), pp. 341–358.
62. A. Dogiaru and R. Carminati, "Electromagnetic field correlations in three-dimensional speckles," Phys. Rep. **559**(10), 1016 (2015).
63. E. Wolf, *Introduction to the Theory of Coherence and Polarization of Light* (Cambridge University, 2007).
64. L. Tchvialeva, T. K. Lee, I. Markhvida, D. I. McLean, and H. Z. H. Lui, "Using a zone model to incorporate the influence of geometry on polychromatic speckle contrast," Opt. Eng. **47**(7), 74201 (2008).
65. P. Elies, L. Bernard, F. Leroy-Brehonnet, J. Cariou, and J. Lotrian, "Experimental investigation of the speckle polarization for a polished aluminium sample," J. Phys. D: Appl. Phys. **30**(1), 29–39 (1997).
66. W. Wang, S. Hanson, and M. Takeda, "Statistics of polarization speckle: theory versus experiment," Proc. SPIE 7388(10), 1117 (2009).
67. L. Tchvialeva, I. Markhvida, and T. K. Lee, "Error analysis for polychromatic speckle contrast measurements," Opt. Lasers Eng. **49**(12), 1397–1401 (2011).